

## Insights into quantum tunneling via a phase-space approach

Chen Chen  and Shuyu Zhou \*

*Key Laboratory for Quantum Optics, Shanghai Institute of Optics and Fine Mechanics, Chinese Academy of Sciences, Shanghai 201800, China*

*and Center of Materials Science and Optoelectronics Engineering, University of Chinese Academy of Sciences, Beijing 100049, China*



(Received 14 November 2023; revised 20 January 2024; accepted 1 March 2024; published 29 March 2024)

Quantum tunneling, as a quintessential quantum phenomenon, has been investigated in detail both theoretically and experimentally. Still, the physical picture of the tunneling process is not intuitive, leading to some confusion and paradoxes. In this paper, we have tried to gain insight into quantum tunneling by a phase-space approach. For this purpose, we scrutinize the evolution of the Wigner distribution during tunneling and derive the energy and momentum spectra by integrating over a segment of phase space. In this way, some of the difficulties and paradoxes in tunneling probability, energy conservation, and tunneling time are given a clearer interpretation. Negative probabilities in the Wigner distribution play a key role in the tunneling process, and the origin of negative probabilities clearly indicates that the volatility of matter underlies the various exotic phenomena involved.

DOI: [10.1103/PhysRevA.109.032227](https://doi.org/10.1103/PhysRevA.109.032227)

### I. INTRODUCTION

Quantum tunneling, one of the most famous phenomena predicted by quantum theory and observed experimentally, has long attracted attention [1–6]. This phenomenon occurs in a variety of physical and chemical processes [2,5–8], including even photosynthesis [7] and nuclear fusion [8]. Additionally, it is also the principle behind some advanced applications such as superconducting quantum interference devices [9–11] and scanning tunneling microscopy [12–14]. These techniques are widely used in condensed matter physics and materials science, for example, to study the diffusion of hydrogen atoms on metallic surfaces [15] and to control the magnetism of nanographenes [16]. Recently, experimental studies of quantum tunneling have been performed in cold atomic systems [17,18] as well as in strong-field and ultrafast laser systems [5,19–23], and some remarkable results have been obtained, including tunneling in the relativistic case.

While quantum tunneling can be fairly well described mathematically, its associated physical picture remains somewhat mysterious. For instance, whether particles with kinetic energy lower than the barrier height is conservation of energy during tunneling, and the rationale behind the shortened tunneling time in the presence of a barrier [4,24]. The reason for this confusion is that tunneling is a quantum interference effect [24]. It is, therefore, essentially a reflection of the wave nature of matter. However, the notion of a particle is often introduced into an intuitive physical depiction. How to give a relatively intuitive physical picture without distorting the physical essence of tunneling is a question worth considering.

The Wigner function serves to portray the quasiprobability distribution of a quantum state within phase space, which

is used successfully in many physical problems [25–30]. Numerous investigations have employed the Wigner function to elucidate the tunneling process, yielding noteworthy insights [31–33]. Diverging from classical probability distributions, the Wigner function can assume negative values, often indicative of nonclassical characteristics [34,35]. Previous research has established a correlation between negative Wigner functions and tunneling phenomena [32,33]. Consequently, we posit that employing the Wigner function facilitates a more lucid physical depiction of the tunneling process.

This paper employs numerical simulations to depict the tunneling process of a Gaussian wave packet through a square barrier, utilizing the Schrödinger equation. Subsequently, the wave function is employed to formulate the Wigner function, revealing the evolution within phase space. The momentum and energy spectra are derived by integrating the phase-space distribution across specific subregions. The results demonstrate the conservation of the total energy of the wave packet during tunneling, although the energy distribution within individual regions undergoes a modification. Remarkably, within the barrier region, the kinetic energy spectrum has a negative probability distribution due to the presence of a negative region in the higher segments of the momentum distribution within the Wigner function. Furthermore, we investigate the effect of having the same momentum distribution but different phase distributions on the tunneling time.

### II. METHOD

Our discussion commences with a physical model based on a single atomic wave packet passing through a square barrier, wherein the wave packet is characterized as a scalar matter wave. The motion of the atom is described by the one-dimensional Schrödinger equation [36]. While the

\*syz@siom.ac.cn

computed wave functions encapsulate all pertinent information, discerning a lucid physical representation of the tunneling process remains challenging. Consequently, we proceed to construct the Wigner distribution from the wave function, thereby delving into a more profound comprehension of the tunneling process through an examination of its phase-space evolution.

### A. Wave-packet tunneling simulation model

To simulate the nonrelativistic wave-packet tunneling through a barrier, we employ the time splitting (TS) scheme [37] to numerically compute the Schrödinger equation. Introducing the subsequent changes of variables enhances the computational approach [38,39], where the left-hand side of the arrow is the true value, and the right-hand side is the dimensionless value and its dimension,

$$t \rightarrow \frac{t}{\omega_m}, \quad a_0 = \sqrt{\frac{\hbar}{m\omega_m}}, \quad x \rightarrow xa_0, \quad p \rightarrow p\frac{\hbar}{a_0},$$

$$\psi \rightarrow \frac{\psi}{a_0^{3/2}}, \quad \Omega \rightarrow \Omega\omega_m, \quad E(\cdot) \rightarrow \hbar\omega_mE_{\beta,\Omega}(\cdot), \quad (1)$$

where  $\omega_m = \min(\omega_x, \omega_y, \omega_z)$  is the minimum trap frequency of a three-dimensional harmonic trap, so the dimensionless Schrödinger equation can be expressed as [40]

$$i\frac{\partial\psi}{\partial t} = \left(-\frac{1}{2}\Delta + V\right)\psi. \quad (2)$$

The initial wave function is a one-dimensional freely evolving Gaussian wave packet in momentum representation [41],

$$\psi(p, \tau) = \frac{1}{(2\pi\sigma_p^2)^{1/4}} e^{-\left(\frac{p-p_0}{2\sigma_p}\right)^2} e^{-i\frac{x_0}{\hbar}(p-p_0)} e^{-i\frac{p^2}{2m\hbar}\tau}.$$

Numerical calculations require the wave function to be in coordinate space, which is determined by the inverse Fourier transform of the above expression,

$$\psi(x, \tau) = \frac{1}{(2\pi\sigma_x^2)^{1/4} \sqrt{1 + i\hbar\tau/(2m\sigma_x^2)}} \times \exp\left[\frac{-(x-x_0)^2}{(2\sigma_x)^2 [1 + i\hbar\tau/(2m\sigma_x^2)]}\right] \times \exp\left[\frac{ip_0}{\hbar}\left(x - \frac{p_0\tau}{2m}\right)\right], \quad (3)$$

where  $\tau$  is the time factor that determines the initial phase distribution of the wave packet,  $p_0$  is the central momentum,  $x_0$  represents the initial position,  $m$  is the particle mass, and  $\sigma_x$  is the initial spreading. Note that in order to make the one-dimensional Schrödinger equation dimensionless, the replacement of the wave function should be  $\psi \rightarrow \psi/a_0^{1/2}$ .

Subsequently, we introduce two operators, denoted as  $A$  and  $B$ , corresponding to the dispersion and potential components, respectively. In this study, we adopt the standard decomposition,  $A = \frac{i}{2}\Delta$ , and  $B = -iV(t, \mathbf{x})$ . The time-dependent partial differential equation (PDE) under con-

sideration is expressed as

$$\partial_t \psi(t, \mathbf{x}) = A\psi(t, \mathbf{x}) + B\psi(t, \mathbf{x}), \quad \psi(0, \mathbf{x}) = \psi_0(\mathbf{x}).$$

For all  $t > 0$  and  $\mathbf{x} \in \mathbb{R}^d$ , we represent the solution as  $\psi(t, \mathbf{x}) = e^{(A+B)t}\psi_0(\mathbf{x})$ . The TS scheme approximates the solution  $\psi$  by splitting the exponential operator  $e^{(A+B)t}$  into the operators  $e^{At}$  and  $e^{Bt}$ . The  $\psi$  is written as

$$\psi(t + \delta t, \mathbf{x}) = e^{(A+B)\delta t}\psi(t, \mathbf{x}) \approx e^{a_1 A\delta t} e^{b_1 B\delta t} \dots e^{a_p A\delta t} e^{b_p B\delta t} \psi(t, \mathbf{x}),$$

where  $\{a_k, b_k\}_{1 \leq k \leq p} \subset \mathbb{R}$  are weights, which are computed in order to obtain an approximation of  $e^{(A+B)\delta t}$  of a given order at a time step  $\delta t \ll 1$  and  $t \in \mathbb{R}^+ := t > 0$ . The Lie ( $a_1 = b_1 = 1$ ) and the Strang ( $a_1 = a_2 = 1/2$  and  $b_1 = 1, b_2 = 0$ ) schemes are the most commonly used TS scheme, which are respectively of order one and two. The notable advantage of the splitting scheme lies in the efficient solvability of the equations associated with the operators  $A$  and  $B$ . As described in Ref. [42], the use of fast Fourier transforms facilitates the solution of the partial differential equation associated with  $A$ . Additionally, the ordinary differential equation linked to  $B$  can be accurately integrated.

### B. Wigner function

We can construct the Wigner function as follows [30],

$$W(x, p) = \frac{1}{\pi\hbar} \int \psi(x+s)\psi^*(x-s)e^{-\frac{2ips}{\hbar}} ds$$

$$= \frac{1}{\pi\hbar} \int \phi(p+q)\phi^*(p-q)e^{\frac{2iqx}{\hbar}} dq, \quad (4)$$

where  $\psi(x)$  and  $\phi(p)$  are the wave functions in the position and the momentum representation, respectively. Such a function satisfies the normalization condition  $\int W(x, p) dx dp = 1$ . Integrating the Wigner function over the whole momentum space gives a density distribution, which is  $\int W(x, p) dp = |\psi(x)|^2$ . Similarly, integrating the Wigner function across the entire coordinate space yields the momentum distribution. The resulting distribution, when integrated over either the complete coordinate or momentum space, is non-negative and measurable. However, if integration is confined to a specific portion of the phase space to obtain the momentum spectrum within that region, the outcome may feature negative values. Classically, negative probabilities are impermissible. From a quantum standpoint, integrating over a parton region of the Wigner distribution can be perplexing. This situation is akin to transforming only a segment of the wave function in coordinate space into a wave function in momentum space through a Fourier transform, lacking a clear physical interpretation. Nevertheless, despite this, integrating over portions of the Wigner distribution can still furnish valuable information, comparable to how the short-time Fourier transform of a signal in the time domain can offer useful insights in the frequency domain. Notably, this perspective depicts the momentum distribution within a partial coordinate space which is similar to the classical standpoint, but the classical view does not allow for negative probabilities.

We define that  $P(p) = \int_{x_1}^{x_2} W(x, p) dx$  is the momentum spectrum in this region, where  $x_1$  and  $x_2$  are the coordinates

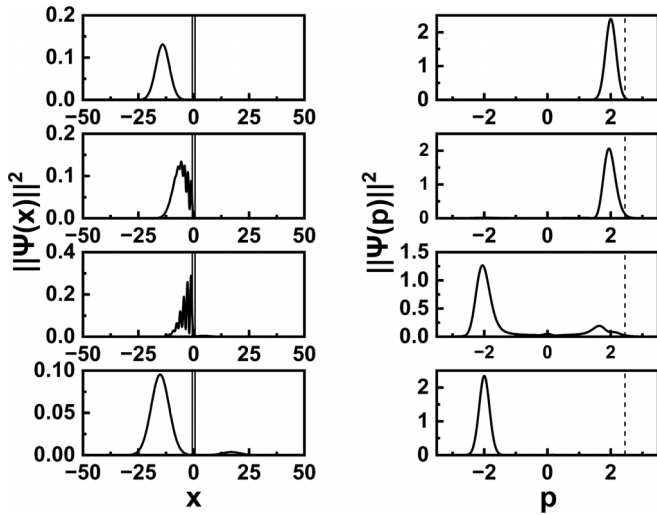


FIG. 1. Four snapshots of a simulated Gaussian wave-packet tunneling process. The left-hand column shows the configuration space probability density, with vertical lines marking the location of the rectangular barrier; on the right is the momentum space probability density, with the dashed line indicating the momentum corresponding to the height of the barrier. From top to bottom, the wave packet is shown: well before it reaches the barrier ( $t = 2.99$ ); just before it enters the barrier ( $t = 5.98$ ); in the midst of the barrier interaction ( $t = 11.47$ ); and just as the interaction ends ( $t = 17.45$ ).

of the starting and ending points of the region, respectively. The kinetic energy spectrum in this region is  $P_T(T) = P(p = \sqrt{2mT}) + P(p = -\sqrt{2mT})$ , and the energy spectrum in this region is  $P_E(E) = P_T(T = E - V)$ .

### III. RESULTS

For our numerical computations, we select the atom  $^{87}\text{Rb}$  with a mass of  $1.443 \times 10^{-25}$  kg. The atom has a central velocity of 1.5 mm/s, an initial position  $x_0$  of  $-20 \mu\text{m}$ , and an initial spread  $\sigma_x$  of  $3 \mu\text{m}$ . It encounters a barrier with 1.5 times the central energy and a width of  $1.6 \mu\text{m}$ . Setting  $\omega_m = 2\pi \times 116$  Hz, the dimensionless parameters of condition I are as follows:

$$\tau = 0, \quad p_0 = 2, \quad x_0 = -20, \quad \sigma_x = 3,$$

$$\frac{V}{E} = 1.5, \quad w_{\text{barrier}} = 1.6.$$

Under condition I, utilizing the procedure outlined in Sec. II A, we obtain the wave-packet distribution in both coordinate and momentum space, depicted in Fig. 1. These distributions bear a resemblance to those presented in Ref. [43]. Following the wave-function computation, we construct the Wigner function using Eq. (4). The phase-space distribution of several representative moments of the tunneling process, considering the specified initial conditions, is illustrated in Fig. 2. For a more detailed description of the evolution of the Wigner distribution during this process, refer to Appendix A. Subsequently, we delve into the characteristics of the wave-packet tunneling through the barrier in three issues.

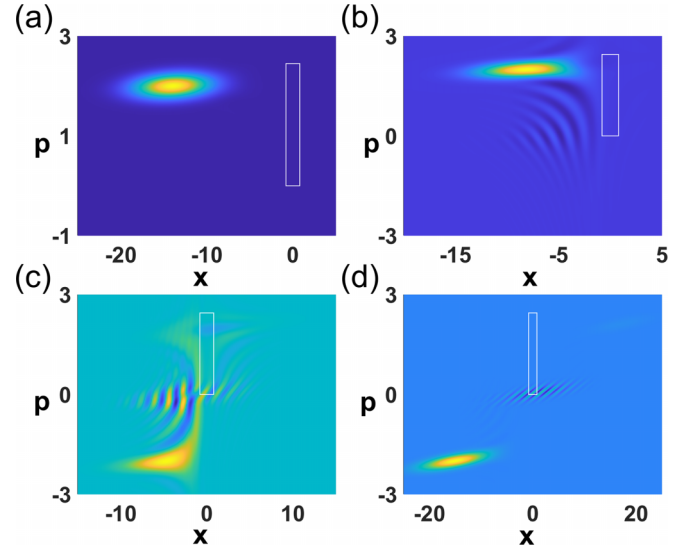


FIG. 2. Evolution of the Wigner distribution of Gaussian wave-packet tunneling. (a)  $t = 2.99$ , (b)  $t = 5.98$ , (c)  $t = 11.47$ , and (d)  $t = 17.45$ .

#### A. Deformation of the phase-space distribution and the tunneling probability

The free evolution of the Wigner function in the absence of an external potential field proceeds according to  $W(x, p, t) = W(x - \frac{p}{m}\delta t, p, t_0)$ , where  $\delta t = t - t_0$  is the evolutionary time [26,28,29]. However, the phase-space distribution is deformed after encountering a barrier. Under condition I, the approaching barrier induces wave-packet deformation, resulting in a broadening of the momentum distribution, as depicted in Fig. 3(a). This broadening affects both the high- and low-energy components, causing an upward shift in the peak position of the distribution. While the total kinetic energy remains approximately constant during the momentum broadening process, the classical sense fraction of barrier crossings increases due to the amplified high-energy segments.

Intuitively, one might easily conceive that the momentum broadening originates from the inherent uncertainty between the momentum and position distributions, given that the barrier constrains the spatial extent of the wave packet. However, this interpretation is not entirely accurate. Let us elucidate this with an example. Under condition II ( $\tau = 0, p_0 = 2, x_0 =$

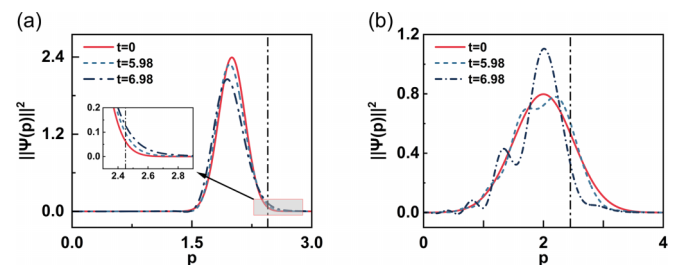


FIG. 3. The probability density of momentum in the incident region (the left of the barrier). (a) For condition I, and (b) for condition II. The vertical dashed line indicates the momentum corresponding to the barrier height.

$-20$ ,  $\sigma_x = 1$ ,  $V/E = 1.5$ ,  $w_{\text{barrier}} = 1.6$ ), the wave packet also undergoes deformation upon approaching the barrier, resulting in changes to both the momentum and spatial distributions. However, the alteration in the momentum distribution leads to a reduced fraction of kinetic energy above the barrier as depicted in Fig. 3(b). Furthermore, the momentum distribution is not simply broadened or narrowed; it exhibits oscillations within the distribution, suggesting that the variation of the distribution can be understood as interference induced by the barrier.

The momentum spectrum within the incident region (i.e., to the left of the barrier) delineates the proportion of the wave packet that can, in the classical sense, traverse the barrier. For condition I: At  $t = 0$  the share on the left-hand side of the barrier is 100.00%, and the fraction of classically allowable crossing is 0.35%. At  $t = 5.9845$ , the left-hand side of the barrier constitutes 99.40% of the share, and the fraction of classically allowed passage increases to 0.75%. By  $t = 6.9819$ , the left-hand side has 97.40% share, and the fraction of classically allowed passage rises to 1.39%. The ultimate tunneling ratio is 4.49%. Consequently, the fraction of classically allowed passage experiences a noteworthy increase as the wave packet encounters the barrier and undergoes deformation under condition I. Contrastingly, for condition II: At  $t = 0$  the share on the left-hand side of the barrier is 100.00% and the classical allowable crossing part is 18.43%. At  $t = 5.9845$ , the left-hand side constitutes 99.03% of the share, and the fraction of classically allowed passage decreases to 16.56%. By  $t = 6.9819$ , the left-hand side has 93.90% share, and the fraction of classically allowed passage further reduces to 6.30%. The final tunneling ratio is 13.50%. In contrast to condition I, the fraction of tunneling allowed under condition II is significantly smaller than the fraction allowed classically.

Remarkably, modifying the momentum spectrum to include more segments above the barrier enhances the likelihood of eventual crossing through the barrier region. Conversely, if the initial alteration in the momentum spectrum leads to a reduction in the portion above the barrier, the final transmission proportionally diminishes compared to the classical transmission of the initial wave packet. Thus, we provide a more intuitive interpretation of the difference between the transmittance of the quantum tunneling process and the classical one.

### B. Conservation of energy

In the classical scenario, when a particle enters the barrier region, energy conservation demands an immediate decrease in kinetic energy to offset the heightened potential energy. Should the kinetic energy of a classical particle be lower than the barrier height, it is precluded from entering the barrier region. In quantum theory, however, particles characterized as wave packets of matter do not undergo abrupt changes at the barrier boundary as in the classical model; instead, they exhibit continuous variation. This raises the pertinent questions: If the kinetic energy of the wave packet entering the barrier region remains roughly constant rather than undergoing an abrupt decrease, the resulting augmented potential energy may lead to energy nonconservation. Alternatively, if the kinetic energy of the wave packet undergoes a sudden

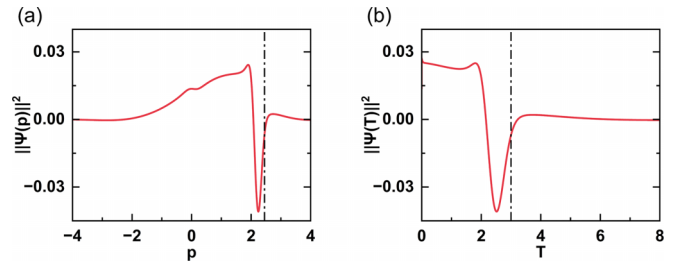


FIG. 4. The momentum and kinetic energy distributions of the wave packet in the barrier region ( $t = 6.98$ ). (a) Momentum spectrum: The vertical dashed line indicates the momentum corresponding to the barrier height. (b) Kinetic energy spectrum: The vertical dashed line indicates the barrier height.

decrease after entering the barrier region, it fails to adhere to the evolution law of the Wigner function. Furthermore, it is commonly understood that the corresponding momentum will decrease, thereby increasing the tunneling time of the wave packet.

However, the evolution of our calculated Wigner function elucidates that the quasiprobability distribution in phase space circumvents the above confusion in a nuanced manner. Initially, the phase-space distribution starts to deform as soon as the wave packet makes contact with the barrier. In particular, in the incident region near the edge of the barrier, there is a broadening towards both the high- and low-momentum regions, and negative probabilities appear in the front of the wave packet between the two extension directions. As the wave packet starts to enter the barrier region, it encompasses both the low- and high-momentum components, thus exhibiting a distribution of kinetic energy from low to high. However, since the region of negative probability is initially located in the higher part of the kinetic energy spectrum, as shown in Fig. 4 (the parameters are the same as condition I), the overall effect is that the total kinetic energy inside the barrier region is smaller than the total potential energy of the wave packet in this region. The sum of the kinetic energy in the incident region, the kinetic energy in the transmitted region, and the potential energy and kinetic energy in the barrier region is equal to the initial kinetic energy of the wave packet, as shown in Table I (the parameters are the same as condition I). Further details on the energy spectra can be found in Appendix B.

The presence of the negative probability region assumes a crucial role. If the probability of the entire phase-space distribution is non-negative, the two conditions, energy

TABLE I. Energy evolution during tunneling.

$t$	$E_{\text{total}}$	$T_{\text{left}}$	$T_{\text{middle}}$	$V_{\text{middle}}$	$T_{\text{right}}$
0	2.014	2.014	0	0	0
3.99	2.014	2.014	0	0	0
5.98	2.014	1.993	0.003	0.018	0
6.98	2.012	1.928	0.008	0.070	0.006
9.97	2.012	1.594	0.025	0.346	0.047
12.47	2.012	1.809	0.010	0.097	0.096
14.96	2.013	1.908	0	0.006	0.099
17.45	2.014	1.914	0	0	0.100

conservation and nonsteep change of the phase-space distribution at the barrier boundary, cannot be simultaneously satisfied. The negative probability region appears in the region with higher momentum (kinetic energy), which effectively reduces the kinetic energy of the barrier region, making the potential energy of the entire interval much higher than the kinetic energy. This approach reflects the conversion of kinetic and potential energy and satisfies the requirement of energy conservation. At the same time, the region of highest momentum does not vanish or lose, which is important for the discussion below.

### C. Tunneling time

The question of how long it takes for a particle to tunnel through a barrier is a long-standing one, and until recently there have been ongoing theoretical and experimental studies in this area [3–5,17,18,24,44]. In quantum theory, particles cannot have both definite positions and velocities, but are described in terms of wave packets. There are various definitions of the tunneling time of a wave packet, the common ones being phase times, dwell time, and Larmor times, among others [4,24]. The phase times, also known as group delays, are derived from the peak position of the incident, reflected, and transmitted wave packets as a function of time. The dwell time is the average time of a particle spending in the barrier, regardless of whether it is ultimately transmitted or reflected. The Larmor times are based on the Larmor precession of a spin in a homogeneous magnetic field, and they are proportional to the time of reflected and transmitted wave packets spend in the barrier region. It was found that the three definitions can be linked by the following formula [24,45],

$$\tau_d = |T|^2 \tau_{gt} + |R|^2 \tau_{gr} - \tau_i, \quad (5)$$

where  $\tau_d$  is the dwell time,  $T$  is the transmission coefficient,  $R$  is the reflection coefficient, and  $\tau_{gt}$  and  $\tau_{gr}$  are transmission and reflection group delays, respectively.  $\tau_i$  is the self-interference delay, which comes from the overlap of incident and reflected waves in front of the barrier. Moreover,  $\tau_T = \tau_{gt} - \tau_i$  and  $\tau_R = \tau_{gr} - \tau_i$  are the Larmor times for transmission and reflection, respectively.

First, we investigate the group delays. In some previous works Gaussian wave packets similar to Eq. (3) are used, but they are usually set as  $\tau = 0$  and  $x_0 = 0$  at the position where the barrier entrance should be [24,44]. In this paper, however, we set three different initial phase times  $\tau$  to observe the effect of the initial phase distribution. We also set different barrier heights and other initial conditions are the same as condition I. Figure 5 depicts the wave packet with and without a barrier under two conditions, normalized by the peak value for ease of comparison ( $t = 22.44$ ). It is evident that the top of the transmitted wave packet is pushed forward in the presence of the barrier. More data on the shifts of the transmitted wave-packet peaks are listed in Table II, where other parameters are the same as condition I, excepting  $\tau$  and  $V/E$ . After the transmitted wave packet moves away from the barrier, the moment at which the peak exits the barrier can be extrapolated from the position and velocity of the peak at a certain time. We can also extrapolate the time that the peak of the incident wave packet would have arrived at the position

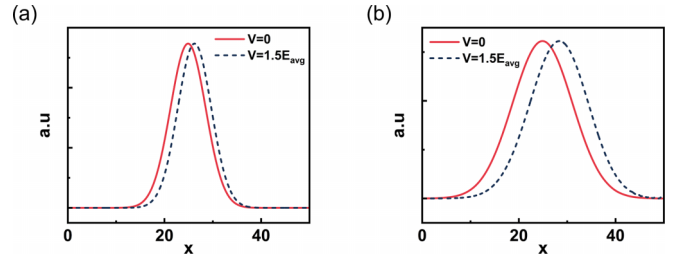


FIG. 5. The shift of the top of the transmitted wave packet in the presence of a barrier. (a)  $\tau = -10$ , and (b)  $\tau = 10$ . Other parameters are the same as condition I.

on the front surface of the barrier in the absence of reflections. The group delay of the transmitted wave packet is obtained by subtracting the latter from the former. In a similar way, we obtain the group delay of the reflected wave packet. Detailed data on the group delays for various conditions are given in Table III. It is easy to find that when the barrier height is higher relative to the kinetic energy of the incident wave packet (such as  $V/E = 1.5$ ), the group delay of the transmitted wave packet is not only significantly shorter than the time required for the same interval when the wave packet propagates freely without a barrier, but also appears negative. This implies the superluminality of the group delay, as the superluminality appears in the Hartman effect [44]. Although the barrier can selectively transmit high-momentum components [1,43], it is not sufficient to explain the significant increase of the group velocity or even the negative group delay of the transmitted wave packet, nor why the group delay is related to the initial phase distribution of the wave packet. In fact, the transmitted wave packet is a reshaping result of the interference of various selectively transmitted momentum components [24,44,46]. Thus, momentum-position correlations caused by the phase distribution of an incident wave packet can have a remarkable effect, which can be clearly seen in phase space. Figure 6 shows the evolution of the Wigner distribution with a different initial phase distribution, where other parameters are the same as condition I. In the case of  $\tau = 10$ , it is the high-momentum part that makes contact with the barrier earlier, since it is in front of the wave packet. In the case of  $\tau = -10$ , the position of the high-momentum part is relatively more backward than in the previous case. Figure 7 shows the momentum spectra of the two cases in the incident region at different times, from which it can be seen that the part with momentum above the barrier appears earlier in the case  $\tau = 10$ . In short, the high-momentum part, which contributes more to the transmitted

TABLE II. The shift of the transmitted peak under various conditions.

$V/E$	$\Delta x_T$	$\Delta x_T$	$\Delta x_T$
	( $\tau = -10$ )	( $\tau = 0$ )	( $\tau = 10$ )
0	0	0	0
0.5	-0.49	-0.38	-0.27
0.8	-0.32	0.16	0.66
1.0	0.15	0.94	1.78
1.3	0.96	2.04	3.13
1.5	1.33	2.43	3.49

TABLE III. The group delays in transmission ( $\tau_{gr}$ ) and in reflection ( $\tau_{gr}$ ) under various conditions.

$V/E$	$\tau_{gr}$ ( $\tau = -10$ )	$\tau_{gr}$ ( $\tau = 0$ )	$\tau_{gr}$ ( $\tau = 10$ )	$\tau_{gr}$ ( $\tau = -10$ )	$\tau_{gr}$ ( $\tau = 0$ )	$\tau_{gr}$ ( $\tau = 10$ )
0	0.80	0.80	0.80	0.00	0.00	0.00
0.5	1.12	1.06	1.01	1.41	2.12	2.81
0.8	1.28	1.04	0.80	1.35	1.71	2.04
1.0	1.21	0.83	0.43	1.19	1.36	1.49
1.3	0.93	0.41	-0.11	0.85	0.89	0.92
1.5	0.75	0.22	-0.28	0.70	0.70	0.72

wave packet, is distributed at the front of the wave packet, which causes the transmitted wave packet to appear earlier and thus the group delay to be negative.

It should be noted that the superluminal group velocity and the negative group delay do not violate the law of causality. The front of the wave packet, which is analogous to the precursor wave of an optical pulse, determines how fast the information travels. We examine the effect of the presence of the barrier on the leading edge of the wave packet, as shown in Fig. 8. The fronts of the transmitted wave packets in various conditions coincide such that the information speed of the transmitted wave packets does not change. It can also be found from Table III that the group delays of reflected and transmitted wave packets are quite different at  $\tau = 0$  and  $\tau = 10$ , but the difference between them is small at  $\tau = -10$ . In the case of  $\tau = -10$ , the wave function approaches that of Eq. (3) with  $\tau = 0$  and  $x_0 = 0$  when the center of the incident wave packet propagates freely (no barrier) to the position where the barrier entrance should be. Thus, the equivalence of the group delays between the transmitted and reflected wave packets requires not only the barrier to be symmetric [24], but

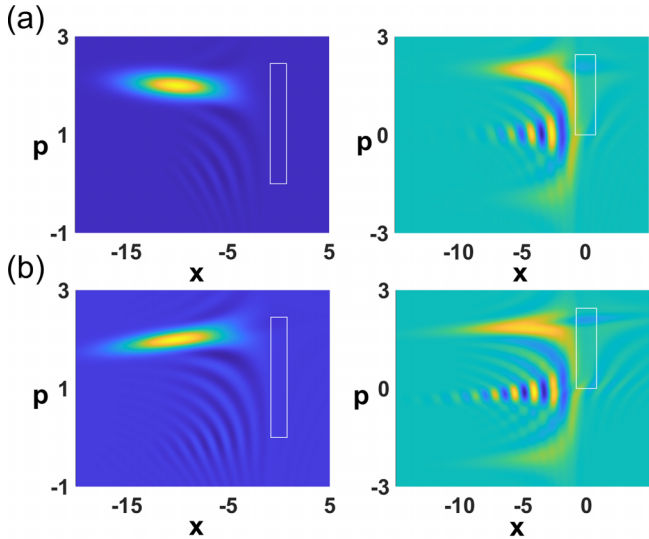


FIG. 6. Evolution of the Wigner distribution with different initial phases. (a)  $\tau = -10$ : The left figure shows the distribution at  $t = 4.99$  and the right figure shows the distribution at  $t = 8.98$ . (b)  $\tau = 10$ : The left figure shows the distribution at  $t = 4.99$  and the right figure shows the distribution at  $t = 8.98$ . Other parameters are the same as condition I.

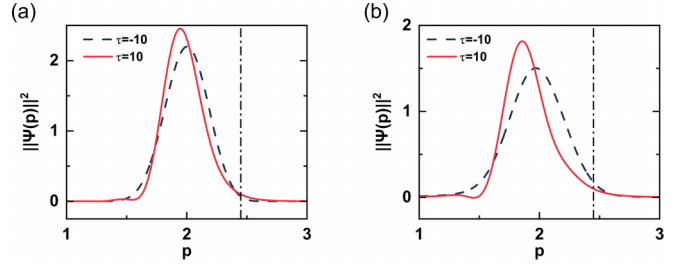


FIG. 7. The momentum spectra of the two cases in the incident region at different times. (a)  $t = 6$ , and (b)  $t = 8$ .

also the phase-space distribution of the incident wave packet to be symmetric as it propagates freely to the site of the barrier entrance.

Then, we examine the dwell time, which is equivalent to an integral over the norm of a time-dependent wave packet over the barrier for all time [47],

$$\tau_d = \int_0^\infty dt \int_0^L dx |\psi(x, t)|^2, \quad (6)$$

where  $[0, L]$  represents the square barrier region in this paper. We calculate the sum of probabilities in the barrier regions as a function of time under different initial phase distributions (other parameters are the same as those in condition I), as shown in Fig. 9. The three curves are different, but they have the same integral value  $\tau_d = 0.469$ .

On the other hand, for rectangular barriers, there is an analytic expression for the dwell time [24],

$$\tau_d(k) = \frac{mL}{2\hbar k(1 + \Delta^2 \tanh^2 \kappa L)} \times \left[ \left(1 + \frac{k^2}{\kappa^2}\right) \frac{\tanh \kappa L}{\kappa L} - \left(\frac{k^2}{\kappa^2} - 1\right) \text{sech}^2 \kappa L \right], \quad (7)$$

where  $\kappa = \sqrt{2m(V - E)}/\hbar$  and  $\Delta = (\kappa/k - k/\kappa)/2$ . This formula can be used when the width of the momentum distribution of the wave packet is very narrow, but for the case in this paper, it is necessary to consider the contribution of the various momentum components of the wave packet, i.e.,

$$\bar{\tau}_d = \int |\psi(k)|^2 \tau_d(k) dk. \quad (8)$$

The dwell time calculated by Eq. (8) under condition I is  $\bar{\tau}_d = 0.462$ , which is fairly close to previously calculated by Eq. (6).

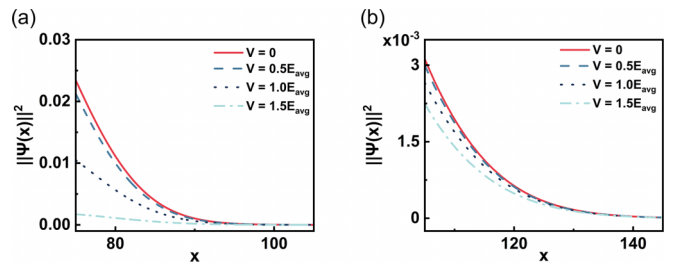


FIG. 8. The front of the transmitted wave packet under various conditions ( $t = 42.39$ ). (a)  $\tau = 10$ , where other parameters are the same as condition I, excepting  $V/E$ , and (b) for condition II, excepting  $V/E$ .

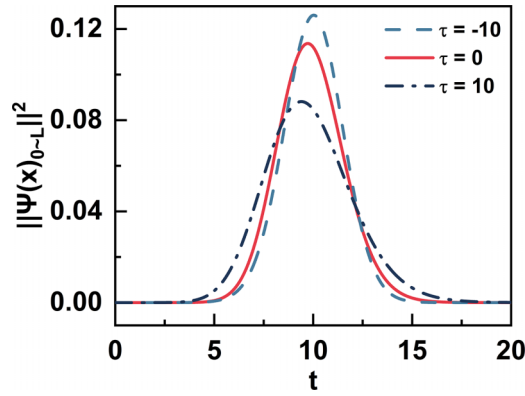


FIG. 9. The sum of probabilities in the barrier regions as a function of time under different initial phase distributions.

Finally, let us verify Eq. (5). To do this, we need to calculate the self-interference delay  $\tau_i$ . For rectangular barriers, there is an analytic expression for the self-interference delay [24].

$$\tau_i(k) = \frac{mL}{2\hbar k(1 + \Delta^2 \tanh^2 \kappa L)} \left[ \left(1 + \frac{\kappa^2}{k^2}\right) \frac{\tanh \kappa L}{\kappa L} \right]. \quad (9)$$

Similar to the calculation of the dwell time, we need to integrate over all momentum components,

$$\bar{\tau}_i = \int |\psi(k)|^2 \tau_i(k) dk. \quad (10)$$

For condition I, the self-interference delay  $\bar{\tau}_i = 0.23$  is calculated according to the method described above. For  $\tau = -10$ , we have  $|T|^2 \tau_{gr} + |R|^2 \tau_{gr} = 0.70$  and Eq. (5) holds in this case. But for  $\tau = 0$  and  $\tau = 10$ , the calculation gives  $|T|^2 \tau_{gr} + |R|^2 \tau_{gr} = 0.68$ . According to the previous calculation, the dwell time does not change with the initial phase parameter  $\tau$  of the wave packet. If Eq. (5) is true, this implies that the self-interference delay  $\tau_i$  depends slightly on the initial phase distribution of the wave packet.

#### IV. DISCUSSION

The previous section showed the existence of negative probability distributions in the momentum or energy spectra obtained when integrating over a part of the phase space, which are essential for clarifying some of the paradoxes in the tunneling process, such as energy conservation. These negative probability distributions on the momentum or energy spectra come from negative values of a quasiprobability Wigner function. Thus, the negative Wigner function is closely related to the nature of quantum tunneling. Hence, it becomes imperative to investigate the conditions under which the negative probability region occurs, or conversely, the conditions under which no negative probability is present. A prior study demonstrated that a sufficient and necessary condition for the Wigner function to be non-negative is that the wave function assumes the form [48]

$$\psi(x) = e^{-\frac{1}{2}(ax^2 + 2bx + c)}, \quad (11)$$

where  $a, b$  are arbitrary complex numbers and  $c$  is the coefficient used for normalization. It is evident that a wave function

of this form corresponds to a Gaussian wave packet with minimal uncertainty in phase space or a deformed Gaussian wave packet. A Gaussian wave packet with minimal uncertainty represents the ground state of a harmonic trap, while a deformed Gaussian wave packet corresponds to its free evolution after release from the trap or its motion in a linear or quadratic potential field after release. For the time evolution of the Wigner function, the pseudoparticle method [26,49] can be employed. The lowest-order (LO) pseudoparticle approximation of the time evolution of the Wigner function divides phase space into cells (pseudoparticles) and tracks the trajectories of these cells using classical equations of motion. It is worth noting that if the potential is a constant, linear, or harmonic oscillator potential, then the LO pseudoparticle method provides the exact solution. In these potentials, the trajectories of the cells in phase space exactly mirror those of classical particles. The cells never overlap with each other, precluding any mutual interference. Consequently, the condition for the Wigner distribution to be non-negative can be interpreted as the existence of an initially non-negative distribution and that the components of the wave packet do not interfere with each other during the evolution. Since the barrier potential field cannot belong to the above three cases, an initially non-negative Gaussian wave packet will definitely develop regions of negative probability in phase space upon contact with the barrier. Reference [33] reveals the close relationship between tunneling and negative quasiprobabilities, while the above discussion shows that negative quasiprobabilities are inevitable as long as there is a barrier. The occurrence of negative probabilities is a sensitive indication of the coherent superposition of the various components in the wave packet under the action of the barrier. Thus, even if the particle picture is preserved to some extent, various singularities in quantum tunneling must be accounted for by considering the wave nature of matter.

The propagation of optical pulses in a dispersive media is similar in nature to the barrier tunneling discussed in this paper. Optical experiments have not only shown the peak advance of the pulse, the superluminality of the group velocity, but also confirmed that the arrival time of the optical precursor wave is always the same, so that causality is not violated [46,50–53]. These studies contribute to the understanding of the properties of quantum tunneling, especially at the tunneling time. On the other hand, matter particles have nonzero rest mass and interact with each other, which is quite different from photons. Therefore, experimental studies of tunneling phenomena in matter particles are still necessary.

Presently, Bose-Einstein condensates (BECs) have been employed to investigate quantum tunneling and related phenomena [17,18]. In contrast to the single-particle wave packets examined in this paper, BECs constitute many-body systems [54,55]. The tunneling behavior of BECs is significantly different from that of single-particle wave packets due to nonlinear effects arising from interatomic interactions. For example, the transmission and tunneling times depend on the positive, negative, and magnitude of interatomic interactions [56,57]. On the other hand, deep cooling techniques developed in microgravity environments in recent years can obtain BECs with picokelvin kinetic energy equivalent temperatures and significantly reduced densities [58,59]. The behavior of BECs under these conditions is very close to

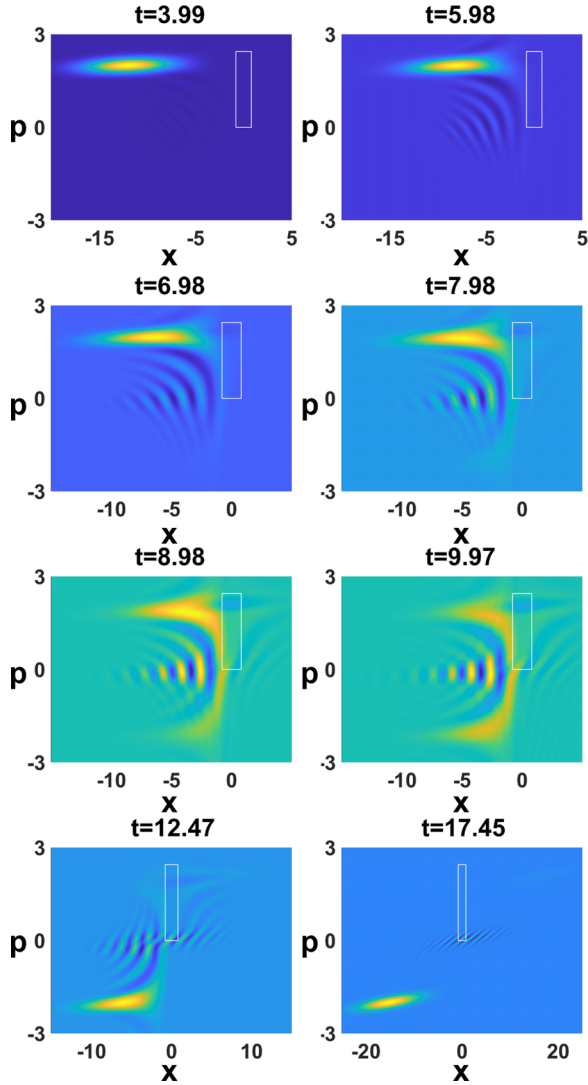


FIG. 10. Evolution of the Wigner distribution under condition I.

that of a single atomic wave packet, so that the experimental results can be compared quantitatively with the theory based on a single atomic wave packet.

## V. CONCLUSION

In summary, we have numerically investigated the quantum tunneling of a Gaussian wave packet through a square barrier. The Wigner distribution is derived from the calculated wave functions and the momentum and energy spectra of a subregion are determined by integrating over a portion of the phase

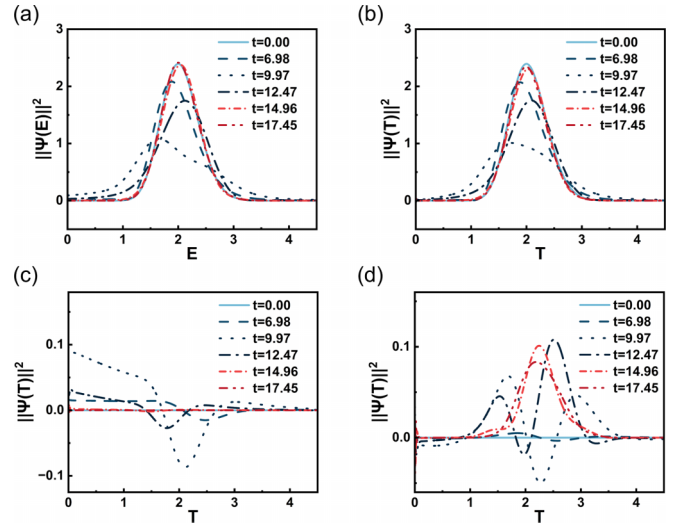


FIG. 11. Kinetic and total energy spectra of the various regions at several moments. (a) The total energy spectra in full space; (b) the kinetic energy spectra in the left region of the barrier; (c) the kinetic energy spectra in the barrier region; (d) the kinetic energy spectra in the right region of the barrier.

space. In this way, we explore in detail the issues of tunneling probability, energy conservation, and tunneling time, and successfully address some of these puzzles and paradoxes. The presence of negative probabilities in the Wigner distribution turns out to be crucial in resolving these problems. Our study enhances the understanding of quantum tunneling and holds implications for applications such as quantum metrology.

## ACKNOWLEDGMENTS

We acknowledge useful discussions with Angang Liang and Bowen Xu. This work was supported by the National Key Research and Development Program of China (No. 2021YFA0718303), and funds provided by the Space Application System of China Manned Space Program.

## APPENDIX A: PHASE-SPACE EVOLUTION

Here, in Fig. 10, we provide a more detailed example of the evolution of the Wigner distribution during tunneling.

## APPENDIX B: ENERGY SPECTRA

Table I exhibits that the sum of the energies in each region remains constant during tunneling, that is, the energy is conserved. Here, in Fig. 11, we show the energy spectrum within each region and as a whole for several moments.

- [1] L. D. Landau and E. M. Lifshitz, *Quantum Mechanics* (Pergamon Press, New York, USA, 1977).
- [2] L. Esaki and Y. Miyahara, A new device using the tunneling process in narrow  $p$ - $n$  junctions, *Solid-State Electron.* **1**, 13 (1960).
- [3] M. Büttiker and R. Landauer, Traversal time for tunneling, *Phys. Rev. Lett.* **49**, 1739 (1982).

- [4] E. H. Hauge and J. A. Støvneng, Tunneling times: a critical review, *Rev. Mod. Phys.* **61**, 917 (1989).
- [5] N. Camus, E. Yakaboylu, L. Fechner, M. Klaiber, M. Laux, Y. Mi, K. Z. Hatsagortsyan, T. Pfeifer, C. H. Keitel, and R. Moshhammer, Experimental evidence for quantum tunneling time, *Phys. Rev. Lett.* **119**, 023201 (2017).

- [6] R. Wild, M. Nötzold, M. Simpson, T. D. Tran, and R. Wester, Tunnelling measured in a very slow ion–molecule reaction, *Nature (London)* **615**, 425 (2023).
- [7] J. Jortner, Temperature dependent activation energy for electron transfer between biological molecules, *J. Chem. Phys.* **64**, 4860 (1976).
- [8] A. B. Balantekin and N. Takigawa, Quantum tunneling in nuclear fusion, *Rev. Mod. Phys.* **70**, 77 (1998).
- [9] V. V. Moshchalkov, L. Gielen, M. Dhallé, C. Van Haesendonck, and Y. Bruynseraede, Quantum interference in a mesoscopic superconducting loop, *Nature (London)* **361**, 617 (1993).
- [10] S.-X. Li, Y. Yu, Y. Zhang, W. Qiu, S. Han, and Z. Wang, Quantitative study of macroscopic quantum tunneling in a dc SQUID: A system with two degrees of freedom, *Phys. Rev. Lett.* **89**, 098301 (2002).
- [11] D. Z. Haxell, E. Cheah, F. Křížek, R. Schott, M. F. Ritter, M. Hinderling, W. Belzig, C. Bruder, W. Wegscheider, H. Riel, and F. Nichele, Measurements of phase dynamics in planar Josephson junctions and SQUIDs, *Phys. Rev. Lett.* **130**, 087002 (2023).
- [12] G. Binnig and H. Rohrer, Scanning tunneling microscopy, *IBM J. Res. Dev.* **44**, 279 (2000).
- [13] C. R. Ast, B. Jäck, J. Senkpiel, M. Eltschka, M. Etzkorn, J. Ankerhold, and K. Kern, Sensing the quantum limit in scanning tunnelling spectroscopy, *Nat. Commun.* **7**, 13009 (2016).
- [14] A. Aishwarya, Z. Cai, A. Raghavan, M. Romanelli, X. Wang, X. Li, G. D. Gu, M. Hirsbrunner, T. Hughes, F. Liu, L. Jiao, and V. Madhavan, Spin-selective tunneling from nanowires of the candidate topological Kondo insulator SmB<sub>6</sub>, *Science* **377**, 1218 (2022).
- [15] L. J. Lauhon and W. Ho, Direct observation of the quantum tunneling of single hydrogen atoms with a scanning tunneling microscope, *Phys. Rev. Lett.* **85**, 4566 (2000).
- [16] C. Zhao, Q. Huang, L. Valenta, K. Eimre, L. Yang, A. V. Yakutovich, W. Xu, J. Ma, X. Feng, M. Juríček, R. Fasel, P. Ruffieux, and C. A. Pignedoli, Tailoring magnetism of graphene nanoflakes via tip-controlled dehydrogenation, *Phys. Rev. Lett.* **132**, 046201 (2024).
- [17] R. Ramos, D. Spierings, I. Racicot, and A. M. Steinberg, Measurement of the time spent by a tunnelling atom within the barrier region, *Nature (London)* **583**, 529 (2020).
- [18] D. C. Spierings and A. M. Steinberg, Observation of the decrease of Larmor tunneling times with lower incident energy, *Phys. Rev. Lett.* **127**, 133001 (2021).
- [19] A. N. Pfeiffer, C. Cirelli, A. S. Landsman, M. Smolarski, D. Dimitrovski, L. B. Madsen, and U. Keller, Probing the longitudinal momentum spread of the electron wave packet at the tunnel exit, *Phys. Rev. Lett.* **109**, 083002 (2012).
- [20] M. Klaiber, E. Yakoboylu, H. Bauke, K. Z. Hatsagortsyan, and C. H. Keitel, Under-the-barrier dynamics in laser-induced relativistic tunneling, *Phys. Rev. Lett.* **110**, 153004 (2013).
- [21] L. Fechner, N. Camus, J. Ullrich, T. Pfeifer, and R. Moshhammer, Strong-field tunneling from a coherent superposition of electronic states, *Phys. Rev. Lett.* **112**, 213001 (2014).
- [22] M. Klaiber, K. Z. Hatsagortsyan, and C. H. Keitel, Under-the-tunneling-barrier recollisions in strong-field ionization, *Phys. Rev. Lett.* **120**, 013201 (2018).
- [23] U. S. Sainadh, H. Xu, X. Wang, A. Atia-Tul-Noor, W. C. Wallace, N. Douguet, A. Bray, I. Ivanov, K. Bartschat, A. Kheifets, R. T. Sang, and I. V. Litvinyuk, Attosecond angular streaking and tunnelling time in atomic hydrogen, *Nature (London)* **568**, 75 (2019).
- [24] H. G. Winful, Tunneling time, the Hartman effect, and superluminality: A proposed resolution of an old paradox, *Phys. Rep.* **436**, 1 (2006).
- [25] E. Wigner, On the quantum correction for thermodynamic equilibrium, *Phys. Rev.* **40**, 749 (1932).
- [26] C.-Y. Wong, Explicit solution of the time evolution of the Wigner function, *J. Opt. B: Quantum Semiclass. Opt.* **5**, S420 (2003).
- [27] U. Leonhardt, *Measuring the Quantum State of Light* (Cambridge University Press, Cambridge, UK, 2005).
- [28] C. Kurtsiefer, T. Pfau, and J. Mlynek, Measurement of the Wigner function of an ensemble of helium atoms, *Nature (London)* **386**, 150 (1997).
- [29] S. Zhou, J. Chabé, R. Salem, T. David, D. Groswasser, M. Keil, Y. Japha, and R. Folman, Phase space tomography of cold-atom dynamics in a weakly corrugated potential, *Phys. Rev. A* **90**, 033620 (2014).
- [30] C. Cohen-Tannoudji, F. Laloë, and B. Diu, *Quantum Mechanics, Vol. 3: Fermions, Bosons, Photons, Correlations, and Entanglement* (Wiley-VCH, Weinheim, Germany, 2019).
- [31] A. M. Kriman, N. C. Kluksdahl, and D. K. Ferry, Scattering states and distribution functions for microstructures, *Phys. Rev. B* **36**, 5953 (1987).
- [32] M. S. Marinov and B. Segev, Quantum tunneling in the Wigner representation, *Phys. Rev. A* **54**, 4752 (1996).
- [33] Y. L. Lin and O. C. O. Dahlsten, Necessity of negative Wigner function for tunneling, *Phys. Rev. A* **102**, 062210 (2020).
- [34] N. Lütkenhaus and S. M. Barnett, Nonclassical effects in phase space, *Phys. Rev. A* **51**, 3340 (1995).
- [35] R. W. Spekkens, Negativity and contextuality are equivalent notions of nonclassicality, *Phys. Rev. Lett.* **101**, 020401 (2008).
- [36] X. Antoine, W. Bao, and C. Besse, Computational methods for the dynamics of the nonlinear Schrödinger/Gross–Pitaevskii equations, *Comput. Phys. Commun.* **184**, 2621 (2013).
- [37] H. Hofstätter, O. Koch, and M. Thalhammer, Convergence analysis of high-order time-splitting pseudo-spectral methods for rotational Gross–Pitaevskii equations, *Numer. Math.* **127**, 315 (2014).
- [38] W. Bao and W. Tang, Ground-state solution of Bose–Einstein condensate by directly minimizing the energy functional, *J. Comput. Phys.* **187**, 230 (2003).
- [39] F. Dalfovo and S. Stringari, Bosons in anisotropic traps: Ground state and vortices, *Phys. Rev. A* **53**, 2477 (1996).
- [40] X. Antoine and R. Duboscq, in *Nonlinear Optical and Atomic Systems: At the Interface of Physics and Mathematics*, edited by C. Besse and J.-C. Garreau (Springer, Cham, 2015), pp. 49–145.
- [41] S. Zhou, C. Chen, B. Xu, A. Liang, Y. Wang, and B. Wang, Characterizing ultra-narrow momentum of atoms by standing-wave light-pulse sequences, *J. Opt. Soc. Am. B* **39**, 3012 (2022).
- [42] X. Antoine and R. Duboscq, GPELab, a Matlab toolbox to solve Gross–Pitaevskii equations II: Dynamics and stochastic simulations, *Comput. Phys. Commun.* **193**, 95 (2015).
- [43] K. Smith and G. Blaylock, Simulations in quantum tunneling, *Am. J. Phys.* **85**, 763 (2017).
- [44] T. E. Hartman, Tunneling of a wave packet, *J. Appl. Phys.* **33**, 3427 (1962).

- [45] H. G. Winful, Delay time and the Hartman effect in quantum tunneling, *Phys. Rev. Lett.* **91**, 260401 (2003).
- [46] L.-G. Wang, N.-H. Liu, Q. Lin, and S.-Y. Zhu, Superluminal propagation of light pulses: A result of interference, *Phys. Rev. E* **68**, 066606 (2003).
- [47] C. R. Leavens and G. C. Aers, Dwell time and phase times for transmission and reflection, *Phys. Rev. B* **39**, 1202 (1989).
- [48] R. Hudson, When is the Wigner quasi-probability density non-negative? *Rep. Math. Phys.* **6**, 249 (1974).
- [49] C.-Y. Wong, Dynamics of nuclear fluid. VIII. Time-dependent Hartree-Fock approximation from a classical point of view, *Phys. Rev. C* **25**, 1460 (1982).
- [50] R. Y. Chiao, Superluminal (but causal) propagation of wave packets in transparent media with inverted atomic populations, *Phys. Rev. A* **48**, R34 (1993).
- [51] R. Y. Chiao and J. Boyce, Superluminality, pareticity, and Earnshaw's theorem in media with inverted populations, *Phys. Rev. Lett.* **73**, 3383 (1994).
- [52] H. He, Z. Hu, Y. Wang, L. Wang, and S. Zhu, Superluminal light propagation assisted by Zeeman coherence, *Opt. Lett.* **31**, 2486 (2006).
- [53] S. Zhang, J. F. Chen, C. Liu, M. M. T. Loy, G. K. L. Wong, and S. Du, Optical precursor of a single photon, *Phys. Rev. Lett.* **106**, 243602 (2011).
- [54] C. J. Pethick and H. Smith, *Bose-Einstein Condensation in Dilute Gases*, 2nd ed. (Cambridge University Press, Cambridge, UK, 2008).
- [55] A. J. Leggett, Bose-Einstein condensation in the alkali gases: Some fundamental concepts, *Rev. Mod. Phys.* **73**, 307 (2001).
- [56] Z. Duan, B. Fan, C.-H. Yuan, J. Cheng, S. Zhu, and W. Zhang, Quantum tunneling time of a Bose-Einstein condensate traversing through a laser-induced potential barrier, *Phys. Rev. A* **81**, 055602 (2010).
- [57] P. Manju, K. S. Hardman, M. A. Sooriyabandara, P. B. Wigley, J. D. Close, N. P. Robins, M. R. Hush, and S. S. Szigeti, Quantum tunneling dynamics of an interacting Bose-Einstein condensate through a Gaussian barrier, *Phys. Rev. A* **98**, 053629 (2018).
- [58] C. Deppner, W. Herr, M. Cornelius, P. Stromberger, T. Sternke, C. Grzeschik, A. Grote, J. Rudolph, S. Herrmann, M. Krutzik, A. Wenzlawski, R. Corgier, E. Charron, D. Guéry-Odelin, N. Gaaloul, C. Lämmerzahl, A. Peters, P. Windpassinger, and E. M. Rasel, Collective-mode enhanced matter-wave optics, *Phys. Rev. Lett.* **127**, 100401 (2021).
- [59] N. Gaaloul, M. Meister, R. Corgier, A. Pichery, P. Boegel, W. Herr, H. Ahlers, E. Charron, J. R. Williams, R. J. Thompson, W. P. Schleich, E. M. Rasel, and N. P. Bigelow, A space-based quantum gas laboratory at picokelvin energy scales, *Nat. Commun.* **13**, 7889 (2022).